Ligand-induced gene activation is associated with oxidative genome damage whose repair is required for transcription

Shiladitya Sengupta[a,1,2,3], Haibo Wang[a,b,1], Chunying Yang[a,4], Bartosz Szczesny[c,d], Muralidhar L. Hegde[a,b,e,2], and Sankar Mitra[a,e,f,2]

[a]Department of Radiation Oncology, Houston Methodist Research Institute, Houston, TX 77030; [b]Department of Neurosurgery, Center for Neuroregeneration, Houston Methodist Research Institute, Houston, TX 77030; [c]Department of Ophthalmology and Visual Sciences, The University of Texas Medical Branch, Galveston, TX 77555; [d]Department of Anesthesiology, The University of Texas Medical Branch, Galveston, TX 77555; [e]Weill Cornell Medical College, Cornell University, New York, NY 10065; and [f]Houston Methodist Cancer Center, Houston Methodist Research Institute, Houston, TX 77030

Edited by Sankar Adhya, National Institutes of Health, National Cancer Institute, Bethesda, MD, and approved July 16, 2020 (received for review November 6, 2019)

Among several reversible epigenetic changes occurring during transcriptional activation, only demethylation of histones and cytosine-phosphate-guanines (CpGs) in gene promoters and other regulatory regions by specific demethylase(s) generates reactive oxygen species (ROS), which oxidize DNA and other cellular components. Here, we show induction of oxidized bases and single-strand breaks (SSBs), but not direct double-strand breaks (DSBs), in the genome during gene activation by ligands of the nuclear receptor superfamily. We observed that these damages were preferentially repaired in promoters via the base excision repair (BER)/single-strand break repair (SSBR) pathway. Interestingly, BER/SSBR inhibition suppressed gene activation. Constitutive association of demethylases with BER/SSBR proteins in multiprotein complexes underscores the coordination of histone/DNA demethylation and genome repair during gene activation. However, ligand-independent transcriptional activation occurring during heat shock (HS) induction is associated with the generation of DSBs, the repair of which is likewise essential for the activation of HS-responsive genes. These observations suggest that the repair of distinct damages induced during diverse transcriptional activation is a universal prerequisite for transcription initiation. Because of limited investigation of demethylation-induced genome damage during transcription, this study suggests that the extent of oxidative genome damage resulting from various cellular processes is substantially underestimated.

transcriptional activation | histone demethylation | DNA demethylation | oxidative genome damage | base excision/single-strand break repair

Chromatin remodeling during transcriptional reprogramming is associated with reversible covalent modifications, primarily acetylation and methylation at specific Lys/Arg residues in histones H3 and H4 and methylation at cytosines (Cs) in cytosine-phosphate-guanine (CpG) dinucleotide clusters in gene regulatory regions (e.g., promoters, enhancers) (1–6). Transcriptional activation involves acetylation of H3/H4 at specific Lys residues, usually in conjunction with the demethylation of H3 at Lys9. At the same time, 5-methyl cytosines (5^mCs) in promoter CpG clusters and other regulatory regions are demethylated. Both protein and DNA demethylases carry out oxidative demethylation and generate reactive oxygen species (ROS) as by-products. Histone demethylases belong to two classes: flavin adenine dinucleotide (FAD)-dependent monoamine oxidases, the founding member being lysine-specific demethylase 1 (LSD1/KDM1A), which generate hydrogen peroxide (H_2O_2), and jumonji (JMJ) family members, which generate superoxide anion ($O_2^{\cdot-}$) during Fe^{2+}/O_2-dependent oxidative decarboxylation of α-ketoglutarate (7–11). Demethylation of 5^mC is carried out by ten-eleven translocation (TET) dioxygenases, which follow the same reaction pathway as the JMJs and thus, generate $O_2^{\cdot-}$; the TETs oxidize 5^mC to 5-hydroxymethyl cytosine ($5^{OH\text{-}m}C$) (12–14). The nuclear ROS generated from these demethylation reactions are distinct from the extranuclear ROS generated primarily as mitochondrial respiration by-products and by various oxidases in the endoplasmic reticulum, peroxisomes, and plasma membrane (15–17). $O_2^{\cdot-}$ is readily converted to H_2O_2 by the ubiquitous superoxide dismutase (18). While H_2O_2 and $O_2^{\cdot-}$ oxidize DNA and other cellular components, these ROS also react with each other in the presence of Fe^{2+} (Haber-Weiss reaction) to form the highly reactive hydroxyl radical, which oxidizes all cellular components, including DNA (19–22).

Here, we demonstrated that these nuclear ROS, generated via histone/CpG demethylation during ligand-induced gene activation, caused DNA base oxidation and single-strand break (SSB), but not direct double-strand break (DSB), in the genome.

Significance

The endogenous genome damage induced by mitochondrial/cytosolic reactive oxygen species (ROS) is well recognized. However, similar damage induced by nuclear ROS generated via histone/cytosine-phosphate-guanine (CpG) demethylation during transcription has not been scrupulously investigated. This report documents the formation of genomic oxidized bases and single-strand breaks during ligand-induced gene activation via histone/CpG demethylation. That repair of these damages occurs preferentially in promoters and is essential for transcriptional activation underscore the essentiality of promoter-specific repair for transcription. In contrast, heat shock (HS) induction generates double-strand breaks, the repair of which is essential for the activation of HS-responsive genes. This study thus implies gross underestimation of endogenous oxidative genome damage and highlights the intrinsic diversity of damage and distinct repair processes associated with transcription.

Author contributions: S.S., M.L.H., and S.M. designed research; S.S., H.W., C.Y., B.S., and M.L.H. performed research; S.S., H.W., C.Y., B.S., M.L.H., and S.M. analyzed data; and S.S. and S.M. wrote the paper.

The authors declare no competing interest.

This article is a PNAS Direct Submission.

[1]S.S. and H.W. contributed equally to this work.

[2]To whom correspondence may be addressed. Email: sengupta.us@gmail.com, mlhegde@houstonmethodist.org, or smitra2@houstonmethodist.org.

[3]Present address: Texas Heart Institute, Houston, TX 77030.

[4]Present address: School of Biomedical Informatics, The University of Texas Health Science Center, Houston, TX 77030.

First published August 21, 2020.

These damages were repaired via the base excision repair (BER)/single-strand break repair (SSBR) pathway (23). We documented the coordination of BER/SSBR with histone/CpG demethylation for promoter-specific repair of these damages during ligand-induced transcriptional activation, in contrast to what we observed during ligand-independent gene activation via heat shock (HS) when double-strand break repair (DSBR) was essential.

Results

Induction of Genome Damage in Diverse Gene Activation Systems. An earlier study documented the generation of 8-oxoguanine (8-oxoG), the most abundant oxidized DNA base lesion, during activation of the B cell lymphoma 2 (BCL2) gene in MCF7 breast cancer line by 17β-estradiol (E2), a ligand for estrogen receptors (24). The formation of 8-oxoG was also observed during Myc-induced transcriptional activation (25). The authors attributed G oxidation by ROS generated specifically during oxidative demethylation of Lys9 methylated histone H3 in the gene promoters. On the basis of these observations, we postulated that diverse ligand-induced transcriptional reprogramming involving the demethylation of histones and CpGs will cause DNA base oxidation and strand break. The induction of genome damage at a global scale followed by their repair can be monitored by comet assay. To study this global damage induction, we selected E2-induced transcriptional activation because thousands of estrogen response elements are most likely present in the genome; the cognate genes would be activated by E2 involving the demethylation of the promoter-bound histones and CpGs (26). Indeed, in alkaline comet assay, we observed global strand breaks after E2 treatment in MCF7 cells (Fig. 1*A*). Moreover, these breaks were transient, indicating their efficient repair within 30 min. These results suggest that such genome damages are tightly coordinated with their repair. To explore the universality of this phenomenon, we stimulated two other cell lines, the human embryonic kidney epithelial line HEK293 and the human nonsmall cell lung adenocarcinoma line A549, with all-trans retinoic acid (RA) and tumor necrosis factor-α (TNFα), respectively. Exposure to RA (Fig. 1*B*) and TNFα (Fig. 1*C*) induced similar global damage, namely strand breaks, followed by their efficient repair. Together, these results strongly suggest that gene activation-linked genome damage and subsequent repair are universal, although each ligand has distinct kinetics of DNA damage induction and repair.

Generation of ROS due to Histone and CpG Demethylation and Induction of Oxidative Genome Damage during Gene Activation. While the ligands used above all generate ROS in cells (27–31), we selected RA for in-depth studies of demethylation-associated oxidative genome damage and repair during gene activation. We used the RA-inducible retinoic acid receptor-β2 (RARβ2) gene activation in HEK293 cells as the model system. First, we confirmed RA-induced generation of ROS by fluorescence-activated cell sorting (FACS) analysis of 2′,7′-dihydrodichlorofluorescin diacetate (H_2-DCFDA) oxidation (Fig. 2*A*) and then showed the generation of both H_2O_2 and $O_2^{\cdot-}$ by colorimetric assays (Fig. 2 *B* and *C*). Together, these observations suggest that RA-induced global transcriptional reprogramming generates ROS, presumably because of histone/CpG demethylation. Using chromatin immunoprecipitation (ChIP) analysis, we then showed that RA reduced the Lys9 dimethylated H3 (H3K9me2) level in the RARβ2 promoter, which contains the retinoic acid response element (RARE) (Fig. 2*D*). Similar reduction of the H3K9me2 level was not observed in a nonspecific region lacking RARE (Fig. 2*D*). Although we observed significant H3K9me2 demethylation not before 60 min of RA treatment, the generation of global strand breaks, estimated by comet assay, peaked at an earlier time point of 15 min (Fig. 1*B*), thereby implying a range of kinetics of histone demethylation and demethylation at other H3/H4 Lys residues (along with CpG demethylation) across the genome, which would account for the early strand breaks. In any event, this result indicates promoter-specific histone demethylation induced by RA, along with the demethylation of 5-methyl CpGs (5^{m}CpGs), as reported elsewhere (32).

Because the alkaline comet assay (Fig. 1) could not distinguish SSBs and DSBs, we used immunofluorescence microscopy to monitor the formation of phosphorylated (Ser 139) histone H2A.X (γH2AX) foci, a marker of DSB induction. The RA-treated cells showed negligible formation of γH2AX foci, compared with the X-ray irradiated (ionizing radiation [IR]; positive control) cells (Fig. 3 *A* and *B*). ChIP analysis also confirmed the negligible formation of γH2AX in the RARβ2 promoter after RA treatment (Fig. 3*C*). These observations indicate that demethylation-linked ROS during RA stimulation for the indicated times do not directly induce DSBs. On the other hand, we

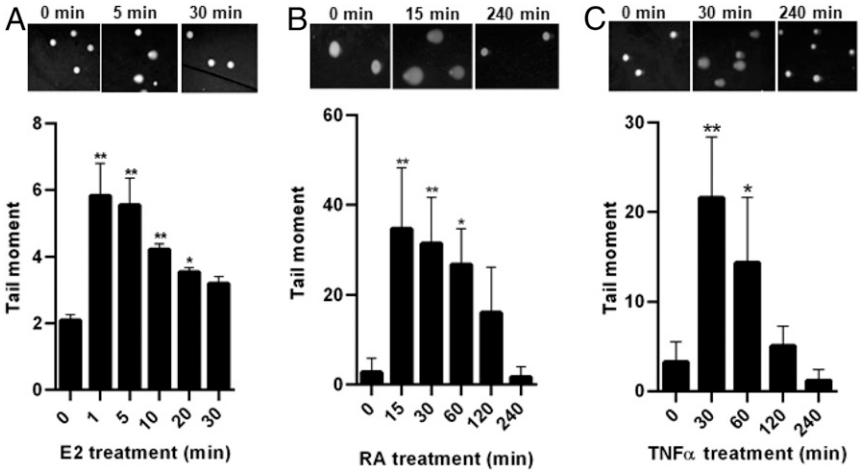

Fig. 1. Comet analysis of ligand-induced strand breaks in cellular genomes. SSBs and DSBs, together with alkali-labile sites, in the genome were estimated by alkaline comet assay in (*A*) MCF7 cells after treatment with 10 nM E2, (*B*) HEK293 cells after treatment with 1 μM RA, and (*C*) A549 cells after treatment with 1 nM TNFα for the indicated times. The mean tail moments of 50 randomly selected cells were calculated from three independent experiments per time point by using the Open Comet/ImageJ program and are shown in the histograms. Representative images are shown. Statistical analysis was performed in GraphPad Prism by using one-way ANOVA with Dunnett's multiple comparisons test. **P* value < 0.05 in *A* and *B* and *P* = 0.0503 in *C*; ***P* value < 0.01.

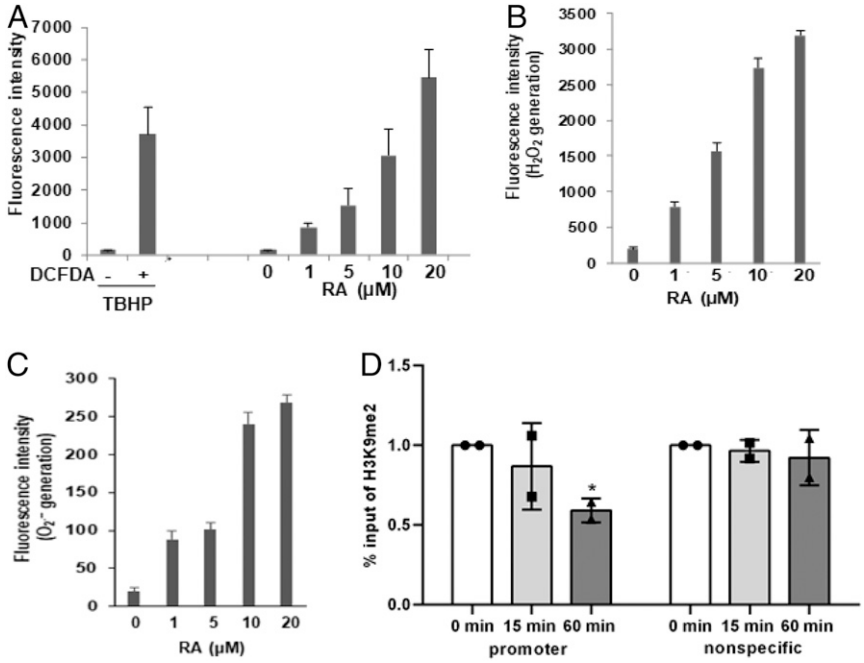

Fig. 2. Analyses of ROS generation and histone demethylation after RA treatment. (*A*) Control and RA-treated HEK293 cells were loaded with nonfluorescent H_2-DCFDA whose oxidation to fluorescent 2′,7′-dichlorofluorescein by ROS was estimated by FACS analysis and plotted as fluorescence intensity (arbitrary units). TBHP (50 μM) was used as a control oxidant. (*B*) HEK293 cells were treated with different doses of RA for 30 min, followed by incubation of the cell culture supernatants with 10-acetyl-3, 7-dihydroxyphenoxazine/horseradish peroxidase (ADHP/HRP), and H_2O_2 generation was measured fluorimetrically (530/590-nm excitation/emission). (*C*) HEK293 cells were incubated with $O_2^{\cdot-}$ staining solution for 1 hr and then treated with ROS inhibitor *N*-acetyl-L-cysteine, followed by treatment with RA for 30 min. The fluorescence intensity was measured by FACS analysis (550/620-nm excitation/emission) to estimate $O_2^{\cdot-}$ generation and plotted. (*D*) Real-time PCR analysis of H3K9me2 ChIP in HEK293 cells showing relative amount of H3K9me2, as fold enrichment of percentage input with respect to IgG, bound to the RARβ2 promoter region (−165 to +82) containing RARE and to a nonspecific region (devoid of RARE) after 15 and 60 min of RA treatment. The data represent the average (with SD) of two or more independent experiments. Statistical analysis was performed in GraphPad Prism by using two-way ANOVA with Tukey's multiple comparisons test. **P* value = 0.0523.

observed a striking increase of 8-oxoG level in the RARβ2 promoter after RA treatment (Fig. 3*D*). Similar increase, also observed elsewhere in the genome (Fig. 3*D*), may be caused by intranuclear diffusion of ROS across the G-rich genomic regions. Interestingly, the 8-oxoG level rapidly decreased selectively in the promoter (Fig. 3*D*). Together, these results imply preferential repair of oxidized bases in promoters. We also examined the kinetics of RA-induced RARβ2 activation (Fig. 3*E*) by measuring the steady-state RARβ2 messenger RNA (mRNA) level by real-time reverse transcription polymerase chain reaction (RT-PCR) assay, which reflected RA-induced RARβ2 transcription. Because optimal RARβ2 transcription occurred after repair completion as suggested by both the comet (Fig. 1*B*) and 8-oxoG ChIP (Fig. 3*D*) analyses, we hypothesized that demethylation and damage repair are coordinated during transcriptional activation and that promoter-specific repair is a prerequisite for transcription.

Association of Demethylases and BER/SSBR Proteins in Chromatin. We speculated that to efficiently coordinate histone/CpG demethylation and repair of the demethylation-induced genome damage, the demethylases and BER/SSBR proteins colocalize in chromatin-bound preformed complexes. We extensively characterized chromatin-bound multiprotein complexes that contained BER/SSBR proteins, along with nonrepair proteins; furthermore, we showed that these complexes were competent in repairing the oxidized bases (33–36). Exposure to ROS increased the stability of these unique complexes, which were distinct for various BER subpathways (23, 34, 35, 37). The complexes were stabilized, independent of DNA binding, via pairwise interaction between the components and could be isolated by size fractionation or after immunoprecipitation (IP) of nuclear extracts (33–35). In the present study, we identified BER/SSBR proteins poly (ADP-ribose) polymerase 1 (PARP1), apurinic/apyrimidinic endonuclease 1 (APE1), polynucleotide kinase phosphatase (PNKP), and DNA polymerase β (DNA Polβ) in the chromatin-bound IPs of a histone demethylase LSD1 and a CpG demethylase TET1, even in the control (RA-untreated) cells (Fig. 4 *A* and *B*). This constitutive association of BER/SSBR proteins in the chromatin-bound LSD1 or TET1 complexes supports our speculation of efficient coordination between histone/CpG demethylation and the repair of the demethylation-induced genome damage. Unexpectedly, we could not detect other BER/SSBR proteins, such as 8-oxoguanine DNA glycosylase 1 (OGG1), Nei-like 1 DNA glycosylase (NEIL1), X-ray repair cross-complementing protein 1 (XRCC1), and DNA ligase 3 (LIG3), in these IPs. The inability to detect these proteins may reflect the sensitivity of detection, which is dependent on many factors, including the quality of antibody and the lability of some complexes. We should also mention that the specific complexes containing repair protein(s) most likely constitute only a very small fraction of the TET1 or LSD1 IPs. In any case, we performed a reciprocal IP with anti-XRCC1 (α-XRCC1) antibody and observed TET1, LSD1, and APE1 (positive control) in the IPs from both control and RA-treated cells (Fig. 4*C*). Moreover, TET1 IP did not pull down proteins of other DNA repair pathways, such as mutL homolog 1 (MLH1) and postmeiotic segregation increased homolog 2 (PMS2) of the mismatch repair pathway and X-ray repair cross-complementing protein 4 (XRCC4), which is involved in the DSBR pathway via nonhomologous end joining (NHEJ) (Fig. 4*D*). These results strongly suggest preferential association of specific BER/SSBR proteins with histone/CpG demethylases, which can repair the oxidized bases and SSBs induced by the demethylases.

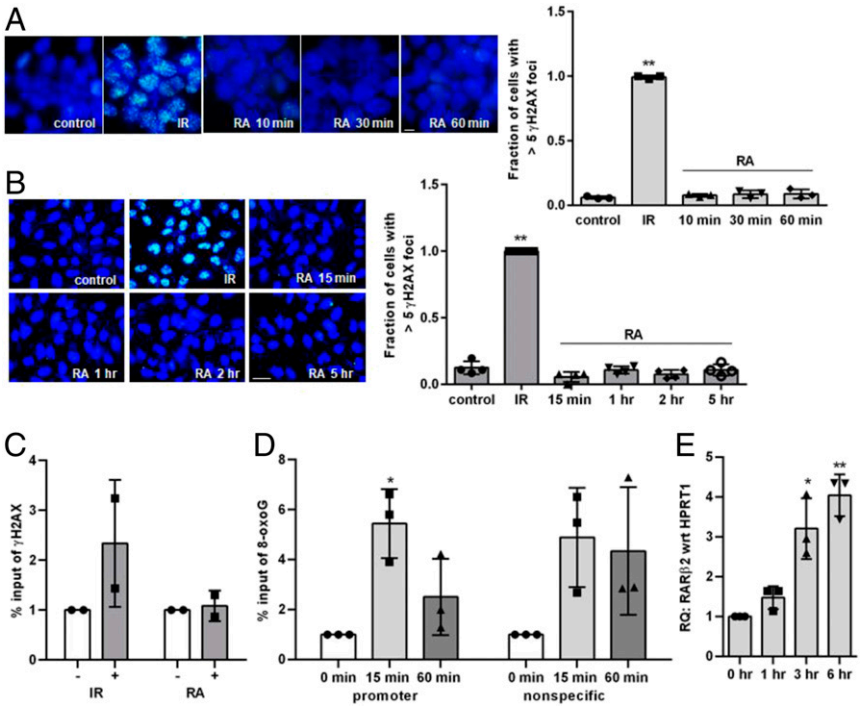

Fig. 3. Induction of base oxidation but not DSB by RA. (*A* and *B*) Immunofluorescence analysis of γH2AX foci was performed in (*A*) HEK293 and (*B*) U2OS cells after 1 μM RA treatment for the indicated times. IR (3-Gy X-rays) was used as a positive control. Representative images are shown, and fraction of cells with more than five foci are plotted. (Scale bars, 10 μm.) (*C*) Real-time PCR analysis of γH2AX ChIP in the RARβ2 promoter in HEK293 cells collected after 15 min of RA treatment or IR. (*D*) Real-time PCR analysis of 8-oxoG ChIP in the RARβ2 promoter and the nonspecific region after RA treatment for the indicated times. (*E*) Real-time RT-PCR analysis of RARβ2 expression as RQ, normalized to HPRT1 expression, in HEK293 cells after 1 μM RA treatment for the indicated times. The data represent the average (with SD) of two or more independent experiments. Statistical analysis was performed in GraphPad Prism by using two-way ANOVA with Tukey's multiple comparisons test. **P* value < 0.05; ***P* value < 0.01.

Essentiality of BER/SSBR Proteins for Ligand-Induced Gene Activation. Our results so far indicate that demethylation and genome damage repair are tightly coupled and raise the possibility that promoter-specific damages are repaired before optimal gene activation. Because intact promoter sequences are necessary for maintaining proper contact with RNA polymerase II in transcription initiation complexes (38, 39), we postulated that promoter-specific repair should be critical for initiating transcription. Hence, we examined whether repair inhibition by down-regulating endogenous BER/SSBR proteins affected RA-induced RARβ2 activation. Down-regulating PARP1 (Fig. 5*A*), XRCC1 (Fig. 5*C*), or PNKP (Fig. 5*D*) by cognate small interfering RNAs (siRNAs) did suppress the level of RARβ2 transcript. Rucaparib, a PARP inhibitor, also suppressed the RARβ2 mRNA level, although moderately, in these cells (Fig. 5*B*).

To further investigate the effect of BER inhibition on RARβ2 transcription, we designed a simple method for measuring the primary transcript level prior to splicing by monitoring a PCR amplicon that picked up an intron and parts of the flanking exons (Fig. 5*E*). We could assess RA-induced RARβ2 transcription by directly quantitating this premRNA amplicon; we observed that the primary transcript level was enhanced after RA treatment (Fig. 5*F*). Consistent with our expectation, BER down-regulation by depleting XRCC1 or inhibiting PARP suppressed the level of this primary transcript, compared with that in the control cells (Fig. 5*G*). Thus, we conclude that BER inhibition did suppress RARβ2 transcription, which was also reflected in the steady-state level of mature mRNA (Fig. 5 *A–D*).

Next, using ChIP analysis, we monitored the relative level of BER/SSBR proteins in the RARβ2 promoter after RA treatment. The amount of SSB-sensor PARP1 and gap-filling DNA Polβ increased as early as 15 min after RA treatment (Fig. 6 *A* and *B*), followed by their release, presumably after completion of the repair. In contrast, RA treatment decreased XRCC1's level in the promoter (Fig. 6*C*). Because of XRCC1's scaffold function in recruiting other BER/SSBR proteins (40, 41), it seems to be constitutively bound to chromatin. RA-induced release of XRCC1 may be necessary for allowing access of the transcription machinery to the promoter after repair completion. LIG3, which forms a stable binary complex with XRCC1 (42, 43), followed similar kinetics of promoter association as XRCC1 after RA treatment (Fig. 6*D*). Together, these results strongly suggest the essentiality of BER/SSBR during gene activation.

DSB Generation and Repair during HS Induction. To examine genome damage and repair during ligand-independent gene activation, we studied gene activation by HS/hyperthermia treatment of HCT116 cells. We observed the formation of γH2AX foci after incubating the cells at 42 °C, reflecting the induction of DSBs, which persisted for at least 24 hr (Fig. 7 *A* and *B*). ChIP analysis showed transient increase of the γH2AX level specifically in the promoter of heat shock protein family A member 4 (HSPA4), an HS-responsive gene (Fig. 7*C*). Interestingly, suppression of the NHEJ-mediated DSBR by a DNA-dependent protein kinase (DNA-PK) inhibitor Nu7441, but not the SSBR by the PARP inhibitor, rucaparib, delayed HS-induced HSPA4 activation (Fig. 7*D*). Thus, in contrast to the predominant role of BER/SSBR pathways during RA-induced RARβ2 activation, hyperthermia induction of HS-responsive genes may involve DSBR via the NHEJ pathway.

Discussion

In this study, we explored the spatiotemporal regulation of global genome damage and repair during transcriptional activation.

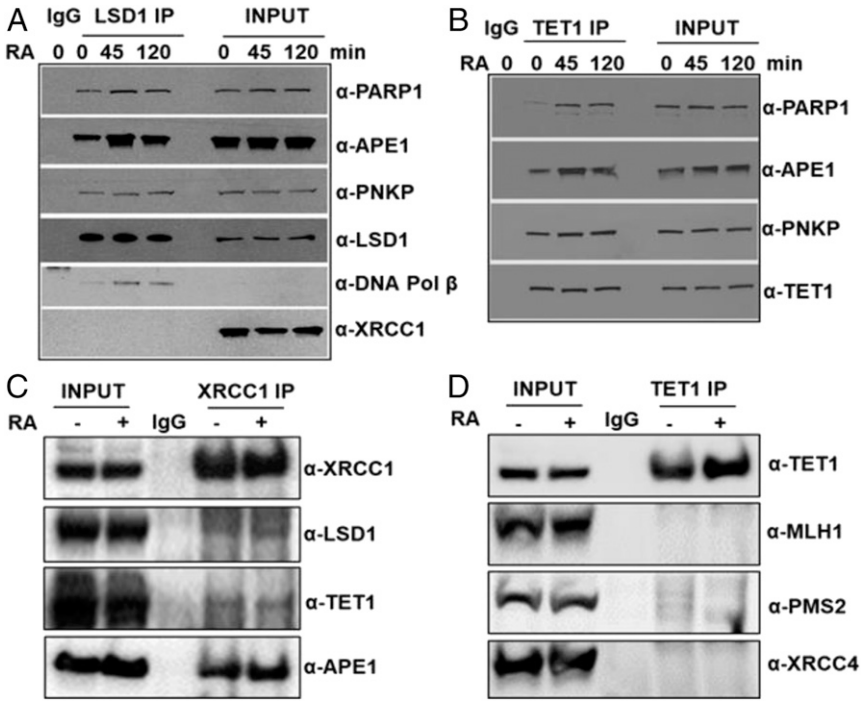

Fig. 4. Constitutive association of BER/SSBR proteins in immunocomplexes of demethylases. (*A* and *B*) Co-IP analysis showing the presence of the indicated BER/SSBR proteins in western blots of chromatin-bound (*A*) LSD1 and (*B*) TET1 IP complexes from control and 1 μM RA-treated HEK293 cells. (*C*) Co-IP analysis showing the presence of LSD1, TET1, and APE1 in the XRCC1 IP from the total nuclear extracts of control and 2-hr 1 μM RA-treated cells. (*D*) Co-IP analysis could not detect non-BER/SSBR proteins, such as MLH1, PMS2, and XRCC4, in the TET1 IP from the total nuclear extracts of control and 2-hr 1 μM RA-treated cells.

The generation of oxidized bases, predominantly 8-oxoG, was observed earlier during E2-induced activation of the BCL2 gene (24). Similar phenomenon, suggesting coordination between the generation of oxidized bases and transcription, was subsequently reported in many studies (25, 44–48). Here, we showed that during ligand-induced gene activation, both oxidized bases and SSBs were generated by ROS, the by-products of histone/CpG demethylation. 8-oxoG, like most other oxidized base lesions, in promoters or gene bodies does not block transcription. In contrast, SSB, generated directly or as a BER intermediate, prevents RNA chain elongation (39, 49). This study showed that the repair of the ligand-induced SSBs in gene promoters was essential for transcription. On the other hand, during ligand-independent gene activation by HS, the DNA topoisomerases, TOP1 and TOP2, are inhibited (50–52), thereby generating persistent SSBs and DSBs, respectively, which also block transcription (53), warranting their prompt repair. Together, these studies, including our study, imply that the damage in promoter sequences not only inhibits transcription (54, 55) but also promotes a transient competition between repair and transcription machineries (56), warranting repair before transcription. Thus, cells use distinct repair systems to remove diverse damages in promoters before transcription initiation.

The direct connection between active CpG demethylation and BER is well established (12, 57–60). The TET-mediated demethylation of 5^{m}CpG generates $5^{OH\text{-}m}$C intermediate. The subsequent DNA demethylation products, 5-formyl C and 5-carboxyl C, are excised by the thymine DNA glycosylase (TDG)/single-strand-selective monofunctional uracil DNA glycosylase 1 (SMUG1) family of BER glycosylases, restoring the unmodified C residue. However, BER/SSBR in repairing the oxidized bases and SSBs induced by the ROS by-products of histone/CpG demethylation has not been scrupulously investigated. Although the generation of oxidized bases and SSBs may be global, here we demonstrated that these damages were preferentially repaired in the promoter region, as a prerequisite for transcriptional activation.

Structural relaxation is essential for DNA transcription in condensed chromatin (61). The TOP1 and TOP2 topoisomerases maintain topological states of chromatinized DNA during DNA transactions (62, 63). The TOP1/TOP2-mediated generation of transient strand breaks releases the topological constraint and favors chromatin looping, thereby facilitating cross-talk between distal enhancers and proximal promoters for transcriptional activation (32, 64). However, the demethylation–ROS-induced strand breaks appear to be detrimental to cellular physiology, until repaired, because these strand breaks are not transient, unlike those generated by TOP1 and TOP2. Our study indicates that the strand breaks generated by ligands do not facilitate transcription, rather inhibit, and their prompt repair is essential for transcription. Additionally, during testosterone-induced activation of androgen receptor target genes, TOP1 generates SSBs, which are required for robust enhancer RNA synthesis and enhancer activation (65), a distinct mechanism of transcriptional activation. Although SSBs might favor chromatin looping for transcription, their repair is essential for restoring promoter sequence integrity needed for transcription initiation. Thus, a dynamic balance exists between the induction of strand breaks, chromatin looping, and transcriptional activation (66–68) where subsequent repair of these breaks seems to be essential.

Accumulating evidence indicates the involvement of DNA repair pathway(s) in transcriptional regulation, particularly where TOP2β-mediated generation of DSBs and the involvement of DSBR during signal-dependent gene activation were shown (69, 70). Such signal-dependent "programmed DNA nicks and strand breaks" may promote both transcriptional initiation and elongation by facilitating the assembly of multiprotein regulatory complexes and chromatin looping (71). In this study, we showed that DSBs were not generated directly by RA. However, DSBs could

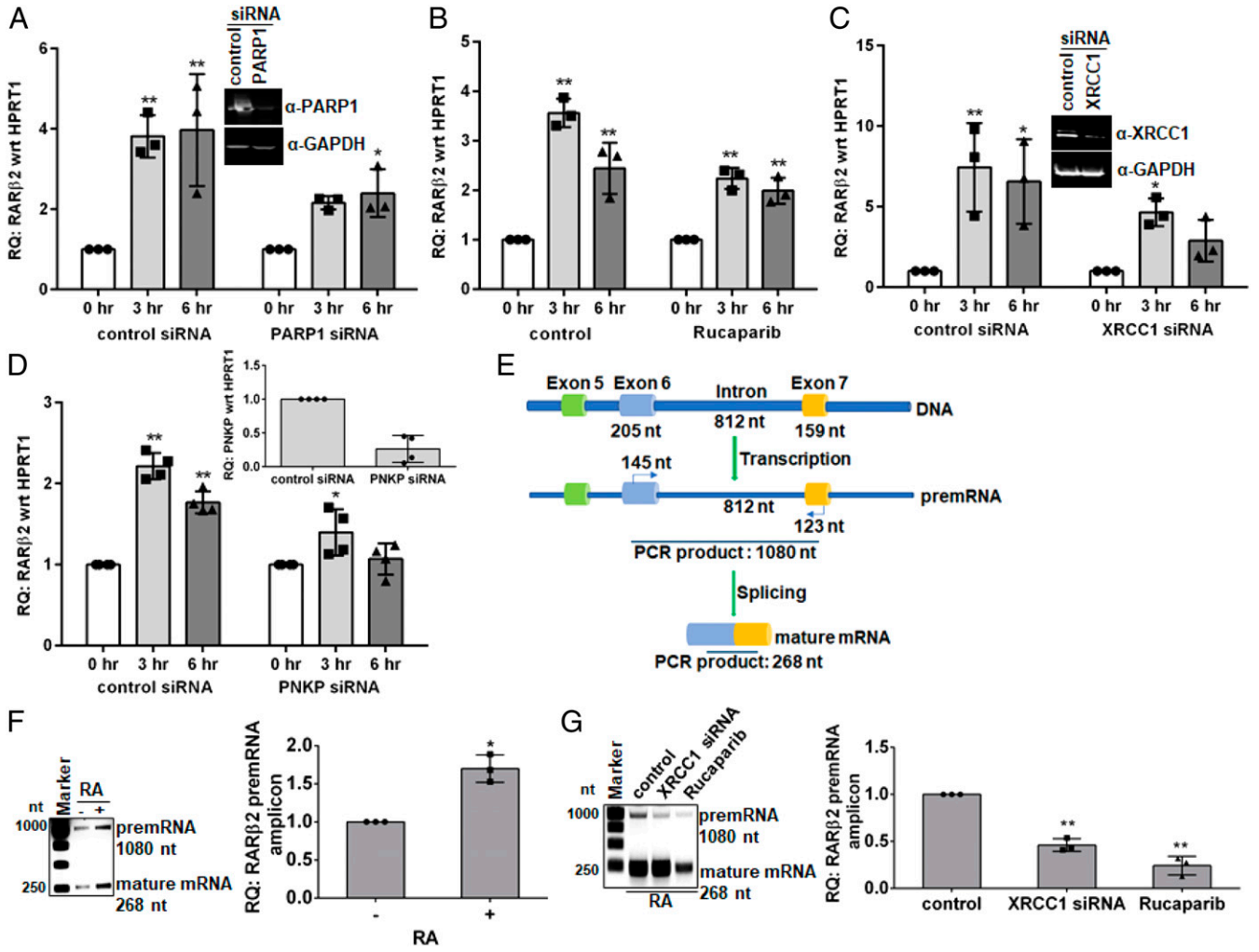

Fig. 5. Suppression of RA-induced RARβ2 activation by BER/SSBR inhibition. (*A–D*) Real-time RT-PCR analysis of RA-induced RARβ2 expression, normalized to HPRT1 expression, in (*A*) PARP1-down-regulated, (*B*) PARP-inhibited, (*C*) XRCC1-down-regulated, and (*D*) PNKP-down-regulated HEK293 cells as a function of time of 1 μM RA treatment. Before RA treatment, down-regulation of PARP1, XRCC1, or PNKP was achieved by 80 nM siRNA via transient transfection for 48 hr, or PARP inhibition was achieved by 1 μM rucaparib treatment for 24 hr. Western blot or real-time RT-PCR analysis was performed to verify the down-regulation of each BER/SSBR protein and is shown in Inset. (*E–G*) RT-PCR analysis of RARβ2 premRNA transcript. (*E*) A schematic of the experimental design showing primer locations and PCR products for amplifying a region of the RARβ2 premRNA and mature mRNA. Ethidium bromide-stained 0.8% agarose gel and the associated ImageJ quantitation showing the PCR products from (*F*) untreated and 3-hr 1 μM RA-treated control cells and (*G*) XRCC1-down-regulated or PARP-inhibited cells, compared with control cells, after RA treatment. The data represent the average (with SD) of three or more independent experiments. Statistical analysis was performed in GraphPad Prism by using two-way ANOVA with Tukey's multiple comparisons test, except in *F* where unpaired *t* test with Welch's correction was used. **P* value < 0.05; ***P* value < 0.01.

be generated during attempted replication of SSB-containing template strands or from bistranded proximal SSBs for which DSBR should be essential to restore promoter integrity. Our study establishes the requirement of BER/SSBR in transcriptional activation. That ROS promote preferential assembly of BER complexes in promoters with open conformation (72), which are vulnerable to oxidation (73), suggests preferential repair of actively transcribing gene promoters via BER/SSBR, consistent with our observations. In a different scenario, the DSBs generated during HS induction are repaired via the NHEJ pathway, which is essential for HS-induced gene activation. Collectively, our study highlights the intrinsic diversity of genome damage mechanisms and distinct repair pathways associated with transcriptional activation.

Egly and coworkers (32) showed that the nucleotide excision repair (NER) proteins, XPG and XPF, were essential for RA-induced RARβ2 activation. They concluded that these nucleases induced DNA strand breaks and promoter CpG demethylation, along with posttranslational modifications of histones. These events promoted CCCTC-binding factor recruitment and chromatin looping as prerequisites for RARβ2 activation. However, we propose an alternative interpretation of their results: RA-induced ROS generate cyclopurines and DNA intrastrand cross-links (74), which should be repaired via NER. Furthermore, the NER proteins involved in both transcription-coupled and global genome NER have regulatory roles in oxidized base repair (75). Thus, ligand-induced gene activation involves the generation of a plethora of genome damages: these damages are repaired by distinct repair complexes to restore promoter integrity needed for transcription initiation.

Transcriptional repression also involves demethylation of histones, but not of CpGs. Specifically, Lys4 trimethylated H3, a marker for transcriptionally active promoters, is demethylated by LSD1 and JMJs (7, 76) during repression. However, because

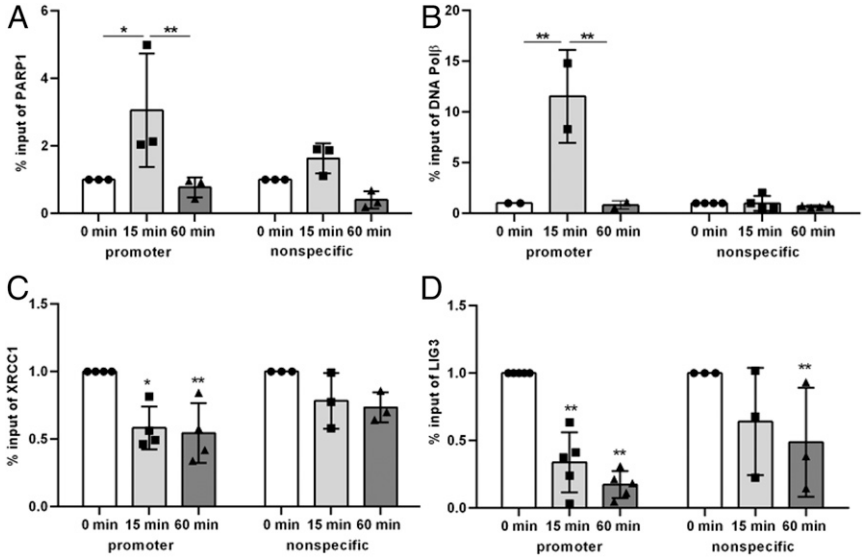

Fig. 6. Association of BER/SSBR proteins with the RARβ2 promoter. Real-time PCR analysis of (*A*) PARP1, (*B*) DNA Polβ, (*C*) XRCC1, and (*D*) LIG3 ChIP in the RARβ2 promoter and the nonspecific region after RA treatment in HEK293 cells. The data represent the average (with SD) of three or more independent experiments. Statistical analysis was performed in GraphPad Prism by using two-way ANOVA with Tukey's multiple comparisons test. **P* value < 0.05; ***P* value < 0.01.

repression does not involve DNA demethylation, the ROS load may be lower during repression than during activation. Thus, it would be interesting to estimate the level of nuclear ROS generated and the extent of genome damage induced during transcriptional activation vs. repression. However, unlike during activation when the repair should precede transcription initiation, repair may not be a prerequisite for repression. In fact, compromised promoter repair may contribute to ligand-induced repression. Thus, future studies exploring differential repair kinetics and complex dynamics that exist across the genomic landscape of active vs. repressed genes should be of significant interest.

Materials and Methods

Cell Lines, siRNAs, Transfection, and Treatment. The human embryonic kidney epithelial HEK293 (ATCC no. CRL-1573), breast adenocarcinoma MCF7 (ATCC no. HTB-22), alveolar adenocarcinoma A549 (ATCC no. CCL-185), and osteosarcoma U2OS (ATCC no. HTB-96) cell lines were maintained in Dulbecco's modified Eagle medium–high-glucose (HyClone) containing 10% fetal calf serum (FCS; Sigma) and antibiotic mixture of 100 IU penicillin and 100 μg/mL streptomycin (Corning) at 37 °C under 5% CO_2 and 95% relative humidity. The human colorectal adenocarcinoma HCT116 (ATCC no. CCL-247) cell line was grown in McCoy's 5A medium (Gibco/Life Technologies) supplemented with FCS and antibiotic mixture. After washing thoroughly in serum-free medium, exponentially growing HEK293 cells were treated with 1 to 10 μM all-trans RA (Sigma; no. R2625), MCF7 cells were treated with 10 nM E2 (Sigma; no. E2257), and A549 cells were treated with 1 nM TNFα (a kind gift of Allan R. Brasier, originally at the University of Texas Medical Branch, Galveston, TX, and currently at the University of Wisconsin, Madison, WI) in the absence of serum for the indicated times for various experiments. HS/hyperthermia treatment was performed by incubating HCT116 cells at 42 °C for the indicated times. Down-regulation of endogenous individual repair proteins was achieved by transiently transfecting exponentially growing cells with specific siRNAs: XRCC1 (77), PARP1 (sense: 5′-GGAUUUUACAGA AACGUGUtt-3′; antisense: 5′-ACACGUUUCUGUAAAAUCCtt-3′), or PNKP (Sigma; no. SASI_Hs01_00067475), along with a universal negative control siRNA (Sigma; no. SIC001). Transfection was performed with Lipofectamine RNAimax (Invitrogen; no. 13778–075) per the manufacturer's protocol (siRNA: 80 nM; Lipofectamine RNAimax: 10 μL per transfection in 3 mL medium). The cells were harvested at 48 hr after transfection, and down-regulation of target genes was verified by western blot analysis or SYBR Green-based real-time RT-PCR analysis. PARP or DNA-PK inhibition was achieved by treating cells with 1 μM rucaparib (Selleckchem; no. S1098) or 10 μM Nu7441 (Sigma; no. 383406), respectively, for 24 hr before RA treatment or HS induction.

Antibodies (α). The following antibodies were used: α-glyceraldehyde 3-phosphate dehydrogenase (GAPDH) (Novus Biologicals; no. NB300-285IR), α-PARP1 (Santa Cruz Biotechnology; no. sc-25780), α-APE1 (Novus Biologicals; no. NB100-116, Cell Signaling; no. 4128), α-PNKP (78), α-DNA Polβ (Proteintech; no. 18003–1-AP, Santa Cruz Biotechnology; no. sc-376581), α-XRCC1 (Neomarkers; no. MS 434-P, Abcam; no. ab134056, Invitrogen; no. MA5-13412), α-LSD1 (Abcam; no. ab17721, Millipore; no. 05–939), α-TET1 (Millipore; no. 09–872, Thermo Fisher Scientific; no. MA5-16312), α-MLH1 (Cell Signaling; no. 3515), α-PMS2 (BD Biosciences; no. 556415), α-XRCC4 (Santa Cruz Biotechnology; no. sc-271087), α-γH2AX (Millipore; no. 05–636-I), and α-8-oxoG (Trevigen; no. 4354-MC-050).

Alkaline Comet Assay. The DNA strand breaks in cells after ligand treatment were analyzed by alkaline comet assay (Comet Assay Kit; Trevigen; no. 4250–050-K) per the manufacturer's protocol. Briefly, control or ligand-treated cells were lysed on comet slides containing low melting agarose and were electrophoresed in alkaline pH. The DNA in the nucleoid was visualized by SYBR Gold staining and imaged with a fluorescence microscope (EVOS FL Auto Imaging System; Life Technologies). The data analysis was performed by using Open Comet/ImageJ (NIH) program in 50 randomly selected cells that were plotted as mean tail moment.

Estimation of Cellular ROS, H_2O_2, and $O_2^{\cdot-}$. The control and RA-treated cells were loaded with nonfluorescent H_2-DCFDA, followed by flow cytometric analysis of 2′,7′-dichlorofluorescein (excitation and emission peaks at 49 and 529 nm, respectively) fluorescence. DCFDA-labeled tert-butyl hydroperoxide (TBHP; 50 μM) was used as a positive control for ROS generation. RA-induced cellular $O_2^{\cdot-}$ and H_2O_2 levels were measured by using the Superoxide Detection Assay Kit (Abcam; no. ab139476) and Hydrogen Peroxide Assay Kit (Cell Biolabs; no. STA-844), respectively, per the manufacturers' instructions.

Subcellular Fractionation. Total nuclear and chromatin extracts were isolated from lysed cells, as previously described (36, 79, 80). In brief, proliferating cells on 10-cm plates at ∼80% confluence were washed in phosphate-buffered saline (PBS), pH 7.4, and then were lysed in cytoplasmic lysis buffer (500 μL per 10-cm plate) containing 10 mM tris(hydroxymethyl)aminomethane.HCl (Tris·HCl), pH 7.9, 0.34 M sucrose, 3 mM $CaCl_2$, 2 mM $MgCl_2$, 0.1 mM ethylenediaminetetraacetic acid (EDTA), 1 mM dithiothreitol, 0.1% Nonidet P-40, and protease inhibitor mixture (Thermo Scientific/Pierce; no. 88666). After centrifugation at 3,500 × *g* for 15 min at 4 °C and discarding the supernatant cytosolic fraction, the nuclear pellets were lysed in nuclear lysis buffer (100 μL per 10-cm plate) containing 20 mM 4-(2-hydroxyethyl)-1-piperazineethanesulfonic acid (Hepes), pH 7.9, 1.5 mM $MgCl_2$, 3 mM EDTA, 150 mM K-acetate, 10% glycerol, 0.5% Nonidet P-40, and protease inhibitor

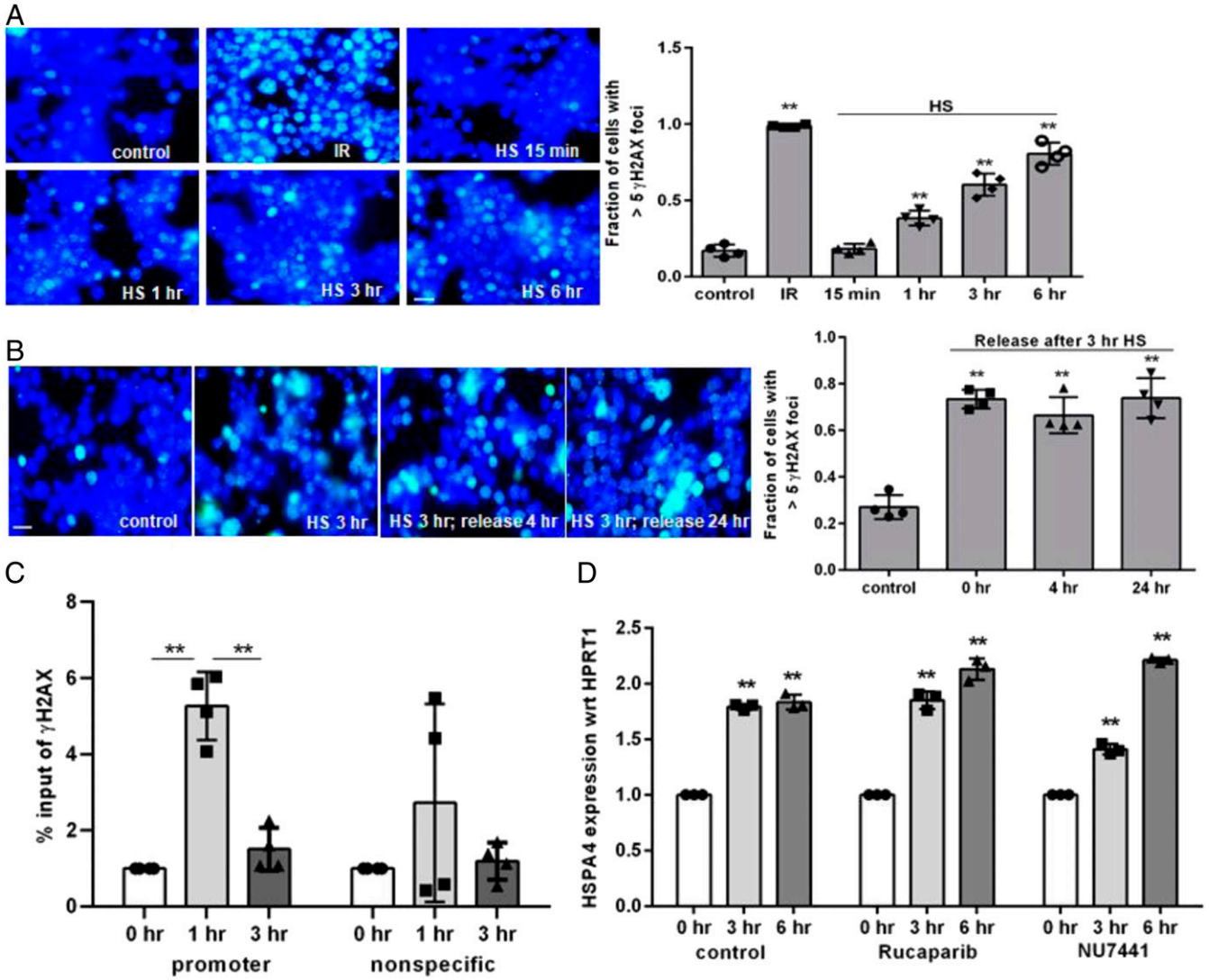

Fig. 7. Generation of DSBs by HS and their repair via NHEJ. (*A* and *B*) Immunofluorescence analysis of γH2AX foci in HCT116 cells (*A*) after HS treatment at 42 °C for the indicated times and (*B*) at the indicated release times at 37 °C after 3-hr HS treatment. Other details are same as in Fig. 3 *A* and *B*. (Scale bars, 10 μm.) (*C*) Real-time PCR analysis of γH2AX ChIP in the HSPA4 gene promoter and in the nonspecific region after HS induction for the indicated times. (*D*) Real-time RT-PCR analysis of HS-induced HSPA4 activation, normalized to HPRT1 expression, in PARP inhibitor (1 μM rucaparib)- or DNA-PK inhibitor (10 μM Nu7441)-treated cells as a function of HS induction time. The data represent the average (with SD) of three or more independent experiments. Statistical analysis was performed in GraphPad Prism by using two-way ANOVA with Tukey's multiple comparisons test. ***P* value < 0.01.

mixture. After vortexing for 15 min at 4 °C, the soluble fractions were separated from the chromatin pellets by centrifugation at 16,000 × *g* for 30 min at 4 °C. To isolate the soluble chromatin extracts, the chromatin pellets were dissolved in chromatin lysis buffer (100 μL per 10-cm plate) containing 150 mM Hepes, pH 7.9, 1.5 mM $MgCl_2$, 150 mM K-acetate, 10% glycerol, and protease inhibitor mixture; incubated with 0.15 units/μL Benzonase (Novagen) at 37 °C for 30 min; and centrifuged at 16,000 × *g* for 30 min at 4 °C. Total cell extracts were isolated by harvesting PBS-washed cells in whole-cell lysis buffer (700 μL per 10-cm plate) containing 50 mM Tris·HCl, pH 7.5, 150 mM NaCl, 1 mM EDTA, 1% Triton X-100, and protease inhibitor mixture. The total soluble extracts were separated from the debris by vortexing for 15 min at 4 °C and centrifuging at 16,000 × *g* for 15 min at 4 °C. To isolate the whole nuclear extracts containing chromatin fractions, nuclear pellets were lysed in 500 μL whole-cell lysis buffer per 10-cm plate. All extracts were stored at −80 °C until use.

Table 1. Primers for real-time ChIP PCR

Real-time ChIP PCR amplicon	Sequence in 5′ to 3′ direction; F: forward primer; R: reverse primer
RARβ2 promoter	F: CTCTGGCTGTCTGCTTTTGC
	R: CATGGGGGAATTCTGGTCCC
HSPA4 promoter	F: TGGCTCGCCTACTTTCTACG
	R: GAATACGTCACGTCCTGGCT
Nonspecific region from chromosome 17	F: TACTATCCCCGTGCTTCCCA
	R: CATTGAGGAGGGGGCAACAT

Table 2. Primers for real time RT-PCR

Real-time RT-PCR amplicon	Sequence in 5′ to 3′ direction; F: forward primer; R: reverse primer
RARβ2 expression	F: AAGTGAGCTGTTCAGAGGCA
	R: AATGCGTTCCGGATCCTACC
HSPA4 expression	F: GCAACAGCAGCAGACACCAGCA
	R: GCCTTCTTGGCTTGGGGTGGT
HPRT1 expression	https://www.realtimeprimers.com/
PNKP expression	https://www.realtimeprimers.com/

Coimmunoprecipitation Analysis. For coimmunoprecipitation (Co-IP) analysis, chromatin extracts and soluble nuclear extracts were precleared by incubation with control immunoglobulin G (IgG) and Magna ChIP protein A/G magnetic beads (Millipore; no. 16–663) for 1 hr at 4 °C with constant shaking. After separating from magnetic beads, the extracts were incubated overnight with 1 μg antibody (α-LSD1, α-TET1, α-XRCC1, or control IgG) per milligram protein in the extracts, together with fresh protein A/G magnetic beads, at 4 °C with constant shaking. The next day, the magnetic beads were washed three times with Tris-buffered saline containing 0.05% Tween 20, followed by sequential washes in low-salt immune complex wash buffer (0.1% sodium dodecyl sulfate [SDS], 1% Triton X-100, 2 mM EDTA, 20 mM Tris·HCl, pH 8, 150 mM NaCl), high-salt immune complex wash buffer (0.1% SDS, 1% Triton X-100, 2 mM EDTA, 20 mM Tris·HCl, pH 8, 500 mM NaCl), LiCl immune complex wash buffer (0.25 M LiCl, 1% Nonidet P-40, 1% Na-deoxycholate, 1 mM EDTA, 10 mM Tris·HCl, pH 8), and TE buffer (10 mM Tris·HCl, 1 mM EDTA, pH 8). Finally, the proteins were eluted from the beads by boiling in Laemmli buffer and were electrophoresed in SDS-polyacrylamide gel for western blot analysis with the appropriate antibodies.

ChIP Analysis. The cells grown to 80% confluence on 10-cm plates were washed in PBS and then cross-linked with 1% formaldehyde in PBS for 15 min at room temperature. After washing three times with PBS, the cells were scraped off the plates in PBS containing protease inhibitor mixture and pelleted at 1,000 × *g* (10 min, 4 °C). The cell pellets were lysed in SDS lysis buffer containing 1% SDS, 10 mM EDTA, 50 mM Tris·HCl, pH 8, and protease inhibitor mixture (1 mL per three 10-cm plates) and incubated on ice for 10 min. The cell lysates were sonicated (XL-2000 QSonica LLC) on ice four to five times at a pulse setting of four with 1-min rest intervals in between and then centrifuged (16,000 × *g*, 15 min, 4 °C) to collect the supernatant containing the sheared chromatin lysate. IP of the chromatin lysates was performed with control IgG or appropriate antibody (5 μg) and 30 μL Magna ChIP Protein A/G magnetic beads. The IP mixture was brought up to 2 mL by 1:10 dilution with ChIP dilution buffer (0.01% SDS, 1.1% Triton X-100, 1.2 mM EDTA, 16.7 mM Tris·HCl, pH 8.1, 167 mM NaCl, protease inhibitor mixture) and incubated overnight at 4 °C with constant shaking. The next day, the IPs were washed sequentially with low-salt wash, high-salt wash, LiCl immune complex wash, and TE buffer. The protein–DNA complexes were subsequently eluted in ChIP elution buffer (1% SDS, 0.1 M $NaHCO_3$), and the cross-linking was reversed by incubation with 200 mM NaCl overnight at 65 °C. The ChIP DNA was purified by sequential incubation with RNase A and proteinase K, followed by phenol chloroform extraction and ethanol precipitation by using the standard protocols. Finally, the DNA was dissolved in 10 mM Tris·HCl, pH 8. The ChIP and 10% input DNA were proceeded to SYBR GREEN-based real-time PCR (7500 Real-Time PCR System; Applied Biosystems) with primers (the primer sequences in the 5′ to 3′ direction are given in Table 1) and SYBR Premix Ex Taq (TaKaRa). The data were represented as percentage input per https://www.thermofisher.com/us/en/home/life-science/epigenetics-noncoding-rna-research/chromatin-remodeling/chromatin-immunoprecipitation-chip/chip-analysis.html.

Real-Time RT-PCR Analysis. Total RNA from control and experimental cells was isolated with the Qiagen RNeasy Mini Kit, including on-column DNase1 digestion, and then processed for complementary DNA (cDNA) synthesis by using the SuperScript III First-Strand Synthesis Kit (Invitrogen; no. 18080051) per the manufacturer's protocol. The expression levels of RARβ2 or HSP4A, along with those of the internal control HPRT1, were analyzed by SYBR GREEN-based real-time RT-PCR. The primer sequences in the 5′ to 3′ direction and other information are given in Table 2. The data were represented as relative quantification (RQ) based on the $2^{-\Delta\Delta CT}$ (CT: cycle threshold) method with the reference samples set at one.

Amplification of PremRNA and Mature mRNA of RARβ2 by PCR. Total RNA was isolated from HEK293 cells by using the RNeasy Mini Kit (Qiagen) per the manufacturer's directions. The cDNA was then synthesized by using the SuperScript III Reverse Transcriptase kit (Invitrogen). Primers (5′ to 3′ sequences: CTTACCCTAAATCGAACTCAGATGCACAA and TTAAGATCTTTGGAA ACATGTGAGGC) were designed for amplification of the RARβ2 premRNA, containing partial exon 6 (145 nt), intron (812 nt), and partial exon 7 (123 nt), and PCR (95 °C for 2 min; 95 °C for 20 s, 56 °C for 40 s, and 65 °C for 90 s for 27 cycles; followed by 65 °C for 6 min) was performed. The PCR product size of the premRNA amplicon (exon 6 + intron + exon 7) is 1,080 nucleotides (nt), and that of the mature mRNA (without the intron) is 268 nt. The PCR products were separated in ethidium bromide-stained 0.8% agarose gel and visualized by the Gel Logic 2200 imagining system (Kodak), followed by quantitation by using ImageJ program.

Immunofluorescence Analysis. The control, RA-treated, or HS-induced cells, plated on chamber slides, were rinsed with PBS and fixed/permeabilized in cold methanol for 10 min. The cells were then incubated with α-γH2AX and diluted (1:1,000) in PBS containing 1% bovine serum albumin (BSA) overnight at 4 °C. The next day, the cells were washed three times with PBS containing 0.1% Tween 20 (PBS-T) and incubated at room temperature in the dark with fluorescence-conjugated secondary antibody diluted (1:500) in 1% BSA for 1 hr. The cells were washed three times with PBS-T, and the slides were mounted by using mounting medium containing 4′,6-diamidino-2-phenylindole (DAPI). Immunofluorescence was visualized in a Zeiss Axio Observer fluorescence microscope (Olympus).

Statistical Analyses. Statistical analyses were performed in GraphPad Prism by using the unpaired *t* test with Welch's correction or one-way or two-way ANOVA with Tukey's or Dunnett's multiple comparisons test on the basis of experimental designs.

Data Availability. All data reported in the text have been compiled in the figures. All materials generated in this study are available upon request.

ACKNOWLEDGMENTS. This work was supported by Cancer Prevention & Research Institute of Texas Training Fellowship CPRIT No. RP101489 (to S.S.); NIH Grants R01 NS088645 (to M.L.H.), RF1 NS112719 (to M.L.H.), R01 GM105090 (to S.M.), R01 CA158910 (to S.M.), and P01 CA092584 (to S.M.); and Houston Methodist laboratory start-up funds (to M.L.H. and S.M.). We thank Dr. Tapas K. Hazra of the University of Texas Medical Branch, Galveston and the members of the laboratories of M.L.H. and S.M. for suggestions during preparation of this manuscript.

1. E. S. Chrun, F. Modolo, F. I. Daniel, Histone modifications: A review about the presence of this epigenetic phenomenon in carcinogenesis. *Pathol. Res. Pract.* **213**, 1329–1339 (2017).
2. C. R. Clapier, B. R. Cairns, The biology of chromatin remodeling complexes. *Annu. Rev. Biochem.* **78**, 273–304 (2009).
3. C. P. Hong, J. Park, T. Y. Roh, Epigenetic regulation in cell reprogramming revealed by genome-wide analysis. *Epigenomics* **3**, 73–81 (2011).
4. T. T. Onder *et al.*, Chromatin-modifying enzymes as modulators of reprogramming. *Nature* **483**, 598–602 (2012).
5. J. R. Edwards, O. Yarychkivska, M. Boulard, T. H. Bestor, DNA methylation and DNA methyltransferases. *Epigenetics Chromatin* **10**, 23 (2017).
6. M. Klutstein, D. Nejman, R. Greenfield, H. Cedar, DNA methylation in cancer and aging. *Cancer Res.* **76**, 3446–3450 (2016).
7. S. M. Kooistra, K. Helin, Molecular mechanisms and potential functions of histone demethylases. *Nat. Rev. Mol. Cell Biol.* **13**, 297–311 (2012).
8. A. Hosseini, S. Minucci, A comprehensive review of lysine-specific demethylase 1 and its roles in cancer. *Epigenomics* **9**, 1123–1142 (2017).
9. H. Alam, B. Gu, M. G. Lee, Histone methylation modifiers in cellular signaling pathways. *Cell. Mol. Life Sci.* **72**, 4577–4592 (2015).
10. R. P. Nowak *et al.*, Advances and challenges in understanding histone demethylase biology. *Curr. Opin. Chem. Biol.* **33**, 151–159 (2016).

11. T. Ismail *et al*., KDM1A microenvironment, its oncogenic potential, and therapeutic significance. *Epigenetics Chromatin* **11**, 33 (2018).
12. X. Wu, Y. Zhang, TET-mediated active DNA demethylation: Mechanism, function and beyond. *Nat. Rev. Genet.* **18**, 517–534 (2017).
13. J. An, A. Rao, M. Ko, TET family dioxygenases and DNA demethylation in stem cells and cancers. *Exp. Mol. Med.* **49**, e323 (2017).
14. P. Melamed, Y. Yosefzon, C. David, A. Tsukerman, L. Pnueli, Tet enzymes, variants, and differential effects on function. *Front. Cell Dev. Biol.* **6**, 22 (2018).
15. S. Choudhary, I. Boldogh, A. R. Brasier, Inside-out signaling pathways from nuclear reactive oxygen species control pulmonary innate immunity. *J. Innate Immun.* **8**, 143–155 (2016).
16. K. M. Holmström, T. Finkel, Cellular mechanisms and physiological consequences of redox-dependent signalling. *Nat. Rev. Mol. Cell Biol.* **15**, 411–421 (2014).
17. M. P. Murphy, How mitochondria produce reactive oxygen species. *Biochem. J.* **417**, 1–13 (2009).
18. Y. Wang, R. Branicky, A. Noë, S. Hekimi, Superoxide dismutases: Dual roles in controlling ROS damage and regulating ROS signaling. *J. Cell Biol.* **217**, 1915–1928 (2018).
19. J. P. Kehrer, The Haber-Weiss reaction and mechanisms of toxicity. *Toxicology* **149**, 43–50 (2000).
20. M. Dizdaroglu, Oxidatively induced DNA damage and its repair in cancer. *Mutat. Res. Rev. Mutat. Res.* **763**, 212–245 (2015).
21. M. Dizdaroglu, P. Jaruga, Mechanisms of free radical-induced damage to DNA. *Free Radic. Res.* **46**, 382–419 (2012).
22. V. B. Djordjević, "Free radicals in cell biology" in *International Review of Cytology: A Survey of Cell Biology*, K. Jeon, Ed. (Academic Press, 2004), Vol. vol. 237, pp. 57–89.
23. M. L. Hegde, T. K. Hazra, S. Mitra, Early steps in the DNA base excision/single-strand interruption repair pathway in mammalian cells. *Cell Res.* **18**, 27–47 (2008).
24. B. Perillo *et al*., DNA oxidation as triggered by H3K9me2 demethylation drives estrogen-induced gene expression. *Science* **319**, 202–206 (2008).
25. S. Amente *et al*., LSD1-mediated demethylation of histone H3 lysine 4 triggers Myc-induced transcription. *Oncogene* **29**, 3691–3702 (2010).
26. V. Bourdeau *et al*., Genome-wide identification of high-affinity estrogen response elements in human and mouse. *Mol. Endocrinol.* **18**, 1411–1427 (2004).
27. T. Miyoshi, T. Arai, K. Yamashita, M. Sasada, T. Uchiyama, NB4 cells treated with all-trans retinoic acid generate toxic reactive oxygen species that cause endothelial hyperpermeability. *Leuk. Res.* **34**, 373–378 (2010).
28. J. Wu, J. M. Hansen, L. Hao, R. N. Taylor, N. Sidell, Retinoic acid stimulation of VEGF secretion from human endometrial stromal cells is mediated by production of reactive oxygen species. *J. Physiol.* **589**, 863–875 (2011).
29. K. C. Fussell, R. G. Udasin, P. J. Smith, M. A. Gallo, J. D. Laskin, Catechol metabolites of endogenous estrogens induce redox cycling and generate reactive oxygen species in breast epithelial cells. *Carcinogenesis* **32**, 1285–1293 (2011).
30. C. H. Woo *et al*., Tumor necrosis factor-alpha generates reactive oxygen species via a cytosolic phospholipase A2-linked cascade. *J. Biol. Chem.* **275**, 32357–32362 (2000).
31. J. J. Kim, S. B. Lee, J. K. Park, Y. D. Yoo, TNF-alpha-induced ROS production triggering apoptosis is directly linked to Romo1 and Bcl-X(L). *Cell Death Differ.* **17**, 1420–1434 (2010).
32. N. Le May, D. Fradin, I. Iltis, P. Bougnères, J. M. Egly, XPG and XPF endonucleases trigger chromatin looping and DNA demethylation for accurate expression of activated genes. *Mol. Cell* **47**, 622–632 (2012).
33. M. L. Hegde, P. M. Hegde, D. Arijit, I. Boldogh, S. Mitra, Human DNA glycosylase NEIL1's interactions with downstream repair proteins is critical for efficient repair of oxidized DNA base damage and enhanced cell survival. *Biomolecules* **2**, 564–578 (2012).
34. M. L. Hegde *et al*., Prereplicative repair of oxidized bases in the human genome is mediated by NEIL1 DNA glycosylase together with replication proteins. *Proc. Natl. Acad. Sci. U.S.A.* **110**, E3090–E3099 (2013).
35. P. M. Hegde *et al*., The C-terminal domain (CTD) of human DNA glycosylase NEIL1 is required for forming BERosome repair complex with DNA replication proteins at the replicating genome: Dominant negative function OF the CTD. *J. Biol. Chem.* **290**, 20919–20933 (2015).
36. S. Sengupta *et al*., Acetylation of oxidized base repair-initiating NEIL1 DNA glycosylase required for chromatin-bound repair complex formation in the human genome increases cellular resistance to oxidative stress. *DNA Repair (Amst.)* **66–67**, 1–10 (2018).
37. M. L. Hegde *et al*., Physical and functional interaction between human oxidized base-specific DNA glycosylase NEIL1 and flap endonuclease 1. *J. Biol. Chem.* **283**, 27028–27037 (2008).
38. K. W. Caldecott, Single-strand break repair and genetic disease. *Nat. Rev. Genet.* **9**, 619–631 (2008).
39. S. D. Kathe, G. P. Shen, S. S. Wallace, Single-stranded breaks in DNA but not oxidative DNA base damages block transcriptional elongation by RNA polymerase II in HeLa cell nuclear extracts. *J. Biol. Chem.* **279**, 18511–18520 (2004).
40. A. Campalans *et al*., XRCC1 interactions with multiple DNA glycosylases: A model for its recruitment to base excision repair. *DNA Repair (Amst.)* **4**, 826–835 (2005).
41. A. Dutta, C. Yang, S. Sengupta, S. Mitra, M. L. Hegde, New paradigms in the repair of oxidative damage in human genome: Mechanisms ensuring repair of mutagenic base lesions during replication and involvement of accessory proteins. *Cell. Mol. Life Sci.* **72**, 1679–1698 (2015).
42. K. W. Caldecott, C. K. McKeown, J. D. Tucker, S. Ljungquist, L. H. Thompson, An interaction between the mammalian DNA repair protein XRCC1 and DNA ligase III. *Mol. Cell. Biol.* **14**, 68–76 (1994).
43. R. A. Nash, K. W. Caldecott, D. E. Barnes, T. Lindahl, XRCC1 protein interacts with one of two distinct forms of DNA ligase III. *Biochemistry* **36**, 5207–5211 (1997).
44. S. Amente, L. Lania, E. V. Avvedimento, B. Majello, DNA oxidation drives Myc mediated transcription. *Cell Cycle* **9**, 3002–3004 (2010).
45. L. Pan *et al*., Oxidized guanine base lesions function in 8-oxoguanine DNA glycosylase-1-mediated epigenetic regulation of nuclear factor κB-driven gene expression. *J. Biol. Chem.* **291**, 25553–25566 (2016).
46. A. M. Fleming, Y. Ding, C. J. Burrows, Oxidative DNA damage is epigenetic by regulating gene transcription via base excision repair. *Proc. Natl. Acad. Sci. U.S.A.* **114**, 2604–2609 (2017).
47. A. M. Fleming, J. Zhu, Y. Ding, C. J. Burrows, 8-Oxo-7,8-dihydroguanine in the context of a gene promoter G-quadruplex is an on-off switch for transcription. *ACS Chem. Biol.* **12**, 2417–2426 (2017).
48. S. Roychoudhury *et al*., Endogenous oxidized DNA bases and APE1 regulate the formation of G-quadruplex structures in the genome. *Proc. Natl. Acad. Sci. U.S.A.* **117**, 11409–11420 (2020).
49. N. Kitsera *et al*., 8-Oxo-7,8-dihydroguanine in DNA does not constitute a barrier to transcription, but is converted into transcription-blocking damage by OGG1. *Nucleic Acids Res.* **39**, 5926–5934 (2011).
50. J. L. Nitiss, Targeting DNA topoisomerase II in cancer chemotherapy. *Nat. Rev. Cancer* **9**, 338–350 (2009).
51. J. L. Nitiss, DNA topoisomerase II and its growing repertoire of biological functions. *Nat. Rev. Cancer* **9**, 327–337 (2009).
52. A. K. Velichko, N. V. Petrova, S. V. Razin, O. L. Kantidze, Mechanism of heat stress-induced cellular senescence elucidates the exclusive vulnerability of early S-phase cells to mild genotoxic stress. *Nucleic Acids Res.* **43**, 6309–6320 (2015).
53. T. Pankotai, E. Soutoglou, Double strand breaks: Hurdles for RNA polymerase II transcription? *Transcription* **4**, 34–38 (2013).
54. R. Ghosh, D. L. Mitchell, Effect of oxidative DNA damage in promoter elements on transcription factor binding. *Nucleic Acids Res.* **27**, 3213–3218 (1999).
55. R. Ghosh, R. Tummala, D. L. Mitchell, Ultraviolet radiation-induced DNA damage in promoter elements inhibits gene expression. *FEBS Lett.* **554**, 427–432 (2003).
56. S. P. Moore, J. Kruchten, K. J. Toomire, P. R. Strauss, Transcription factors and DNA repair enzymes compete for damaged promoter sites. *J. Biol. Chem.* **291**, 5452–5460 (2016).
57. N. Bhutani, D. M. Burns, H. M. Blau, DNA demethylation dynamics. *Cell* **146**, 866–872 (2011).
58. M. S. Kim *et al*., DNA demethylation in hormone-induced transcriptional derepression. *Nature* **461**, 1007–1012 (2009). Correction in: *Nature* **480**, 132 (2011).
59. W. A. Pastor, L. Aravind, A. Rao, TETonic shift: Biological roles of TET proteins in DNA demethylation and transcription. *Nat. Rev. Mol. Cell Biol.* **14**, 341–356 (2013).
60. K. Williams, J. Christensen, K. Helin, DNA methylation: TET proteins-guardians of CpG islands? *EMBO Rep.* **13**, 28–35 (2011).
61. Y. Lorch, R. D. Kornberg, Chromatin-remodeling and the initiation of transcription. *Q. Rev. Biophys.* **48**, 465–470 (2015).
62. J. C. Wang, Cellular roles of DNA topoisomerases: A molecular perspective. *Nat. Rev. Mol. Cell Biol.* **3**, 430–440 (2002).
63. Y. Pommier, Y. Sun, S. N. Huang, J. L. Nitiss, Roles of eukaryotic topoisomerases in transcription, replication and genomic stability. *Nat. Rev. Mol. Cell Biol.* **17**, 703–721 (2016).
64. W. Deng, G. A. Blobel, Do chromatin loops provide epigenetic gene expression states? *Curr. Opin. Genet. Dev.* **20**, 548–554 (2010).
65. J. Puc *et al*., Ligand-dependent enhancer activation regulated by topoisomerase-I activity. *Cell* **160**, 367–380 (2015).
66. L. Baranello *et al*., RNA polymerase II regulates topoisomerase 1 activity to favor efficient transcription. *Cell* **165**, 357–371 (2016).
67. F. Kouzine *et al*., Transcription-dependent dynamic supercoiling is a short-range genomic force. *Nat. Struct. Mol. Biol.* **20**, 396–403 (2013).
68. F. Kouzine, S. Sanford, Z. Elisha-Feil, D. Levens, The functional response of upstream DNA to dynamic supercoiling in vivo. *Nat. Struct. Mol. Biol.* **15**, 146–154 (2008).
69. B. G. Ju *et al*., A topoisomerase IIbeta-mediated dsDNA break required for regulated transcription. *Science* **312**, 1798–1802 (2006).
70. M. C. Haffner, A. M. De Marzo, A. K. Meeker, W. G. Nelson, S. Yegnasubramanian, Transcription-induced DNA double strand breaks: Both oncogenic force and potential therapeutic target? *Clin. Cancer Res.* **17**, 3858–3864 (2011).
71. J. Puc, A. K. Aggarwal, M. G. Rosenfeld, Physiological functions of programmed DNA breaks in signal-induced transcription. *Nat. Rev. Mol. Cell Biol.* **18**, 471–476 (2017).
72. R. Amouroux, A. Campalans, B. Epe, J. P. Radicella, Oxidative stress triggers the preferential assembly of base excision repair complexes on open chromatin regions. *Nucleic Acids Res.* **38**, 2878–2890 (2010).
73. D. W. Clark, T. Phang, M. G. Edwards, M. W. Geraci, M. N. Gillespie, Promoter G-quadruplex sequences are targets for base oxidation and strand cleavage during hypoxia-induced transcription. *Free Radic. Biol. Med.* **53**, 51–59 (2012).
74. B. R. Berquist, D. M. Wilson 3rd, Pathways for repairing and tolerating the spectrum of oxidative DNA lesions. *Cancer Lett.* **327**, 61–72 (2012).
75. J. P. Melis, H. van Steeg, M. Luijten, Oxidative DNA damage and nucleotide excision repair. *Antioxid. Redox Signal.* **18**, 2409–2419 (2013).
76. A. Chicas *et al*., H3K4 demethylation by Jarid1a and Jarid1b contributes to retinoblastoma-mediated gene silencing during cellular senescence. *Proc. Natl. Acad. Sci. U.S.A.* **109**, 8971–8976 (2012).
77. A. Dutta *et al*., Microhomology-mediated end joining is activated in irradiated human cells due to phosphorylation-dependent formation of the XRCC1 repair complex. *Nucleic Acids Res.* **45**, 2585–2599 (2017).
78. M. Fanta *et al*., Production, characterization, and epitope mapping of monoclonal antibodies against human polydeoxyribonucleotide kinase. *Hybridoma* **20**, 237–242 (2001).
79. O. Aygün, J. Svejstrup, Y. Liu, A RECQ5-RNA polymerase II association identified by targeted proteomic analysis of human chromatin. *Proc. Natl. Acad. Sci. U.S.A.* **105**, 8580–8584 (2008).
80. C. Yang *et al*., Regulation of oxidized base damage repair by chromatin assembly factor 1 subunit A. *Nucleic Acids Res.* **45**, 739–748 (2017).